



Original Paper

Geological-engineering comprehensive evaluation model and application of feasibility of hydraulic fracturing in hydrate-bearing sediments



Tian-Kui Guo ^{a, b, *}, Lin-Rui Xue ^{a, b}, Ming Chen ^{a, b}, Bo Zhang ^{a, b}, Zhen-Tao Li ^c,
Wen-Jie Huang ^{a, b}, Xiao-Qiang Liu ^d, Zhan-Qing Qu ^{a, b}

^a School of Petroleum Engineering, China University of Petroleum (East China), Qingdao, 266580, Shandong, China

^b State Key Laboratory of Deep Oil and Gas, China University of Petroleum (East China), Qingdao, 266580, Shandong, China

^c AL WAHA Petroleum Co., Ltd., Iraq

^d School of Energy Resources, China University of Geosciences (Beijing), Beijing, 100083, China

ARTICLE INFO

Article history:

Received 10 July 2024

Received in revised form

6 December 2024

Accepted 8 December 2024

Available online 10 December 2024

Edited by Yan-Hua Sun

Keywords:

Hydraulic fracturing

Hydrates

Fracability evaluation

Comprehensive fracability index

Fracability chart

ABSTRACT

Natural gas hydrates (hereinafter referred to as hydrates) are a promising clean energy source. However, their current development is far from reaching commercial exploitation. Reservoir stimulation technology provides new approaches to enhance hydrate development effectiveness. Addressing the current lack of quantitative and objective methods for evaluating the fracability of hydrate reservoirs, this study clarifies the relationship between geological and engineering fracability and proposes a comprehensive evaluation model for hydrate reservoir fracability based on grey relational analysis and the criteria importance through intercriteria correlation method. By integrating results from hydraulic fracturing experiments on hydrate sediments, the fracability of hydrate reservoirs is assessed. The concept of critical construction parameter curves for hydrate reservoirs is introduced for the first time. Additionally, two-dimensional fracability index evaluation charts and three-dimensional fracability construction condition discrimination charts are established. The results indicate that as the comprehensive fracability index increases, the feasibility of forming fractures in hydrate reservoirs improves, and the required normalized fracturing construction parameters gradually decrease. The accuracy rate of the charts in judging experimental results reached 89.74%, enabling quick evaluations of whether hydrate reservoirs are worth fracturing, easy to fracture, and capable of being fractured. This has significant engineering implications for the hydraulic fracturing of hydrate reservoirs.

© 2025 The Authors. Publishing services by Elsevier B.V. on behalf of KeAi Communications Co. Ltd. This is an open access article under the CC BY-NC-ND license (<http://creativecommons.org/licenses/by-nc-nd/4.0/>).

1. Introduction

Natural gas hydrate (hereinafter referred to as hydrate) is a cage-like crystalline compound that exists in low-temperature and high-pressure environments (Sloan, 2003). It mainly occurs in sand and silty clay sedimentary layers. According to preliminary estimates, the amount of natural gas resources existing in hydrates has reached $3 \times 10^{15} \text{ m}^3$, which is regarded as the most potential clean energy source to replace conventional oil and natural gas resources in the 21st century (Sun et al., 2023). Therefore, the development

and utilization of hydrates is of great significance to optimizing the energy structure and improving the climate environment (Cheng et al., 2023).

In the past 30 years, research on the development of hydrate resources has achieved outstanding results, and 11 trial-production tests have been carried out on the hydrate reservoir worldwide (Kurihara et al., 2010; Schoderbek et al., 2013; Yamamoto et al., 2014; Chen et al., 2018; Liu et al., 2023), but there is still a gap between gas production and the threshold for commercial development of hydrates (Chen et al., 2022). Taking the hydrates in the Shenhu Sea area as an example, indoor core permeability test results show that the absolute permeability of the hydrate reservoir is mostly lower than 10 mD (Wei et al., 2021), which greatly inhibits the transmission of pressure drop and the flow of fluids, hindering

* Corresponding author.

E-mail address: guotiankui@upc.edu.cn (T.-K. Guo).

hydrate decomposition and gas production (Wang et al., 2018). Therefore, the key to the mining method of hydrate sediments is to greatly improve the seepage capacity of the hydrate sediment layer and expand the scope of hydrate decomposition.

In recent years, some scholars have proposed the idea of using hydraulic fracturing technology to transform reservoirs to increase hydrate production capacity. They have also conducted preliminary studies of the fracturing characteristics of hydrate sediments through indoor experiments and numerical simulations, confirming the fracability of hydrate deposits (Too et al., 2018; De Silva et al., 2019; Liu et al., 2021, 2022a; Sun et al., 2021; Ge et al., 2023). Ito et al. (2008) conducted hydraulic fracturing experiments on unconsolidated samples of sand-mud interbeds, and found that at low injection rates, single fractures were mainly generated, while at high injection rates, branch fractures were easily formed. Konno et al. (2016) carried out hydraulic fracturing experiments on sandy deposits with a gas hydrate saturation of 72% in a triaxial pressure vessel, and found that the initiation pressure was higher than the minimum principal stress by 2.9–3.9 MPa, and the permeability of the samples significantly increased after fracturing. Too et al. (2018) observed vertical fractures along the axis of the injection pipe in the injection experiments of sandy hydrate samples. Zhang et al. (2020) prepared experimental samples that could simulate hydrate formations in permafrost regions of Alaska. The results showed that compared to unconsolidated pure sand samples, the initiation pressure of hydrated sand samples was higher, and complex fractures were easily formed under high viscosity fracturing fluids. Yang et al. (2020) found that under the combined influence of fluid pressure and thermal stress, there was a delayed effect in fracture propagation in hydrate sediments. Sun et al. (2021) found that regardless of the existence of confining pressure, mud-rich sandy hydrate sediments could form single-wing fractures, and there were two fracturing stages of tensile fracture and erosion. Ma et al. (2022) investigated the pseudo-triaxial fracturing behavior of mud-rich sandy sediments containing ice or hydrates, and found that macroscopic fractures could still be formed even with hydrate saturation as low as 25%–32%. Lu et al. (2021) found that under high confining pressure, mud-rich sandy hydrate sediments exhibited stronger plasticity and wider fractures. The above experiments preliminarily demonstrated the fracability of hydrate sediments. However, existing experimental research is still in the stage of phenomenological analysis, lacking quantitative evaluation of the fracability of hydrates under the comprehensive action of multiple factors.

Existing reservoir fracability assessments mainly focus on shale reservoirs (Guo et al., 2015; Qu et al., 2017). Chong et al. (2010) first proposed the use of quantified values of rock brittleness to characterize the fracability of reservoirs, where a higher brittleness index indicates that the reservoir is more prone to fracturing under external forces. According to research statistics, there are approximately more than twenty methods for calculating brittleness index (Yagiz, 2006; Rick et al., 2008; Guo et al., 2017), including strength-based brittleness evaluation methods, hardness or firmness-based brittleness evaluation methods, and brittleness evaluation methods based on full stress-strain curve analysis, among others. Among them, Young's modulus and Poisson's ratio are two important mechanical parameters for calculating brittleness index, which are closely related to the brittleness of rocks (Rick et al., 2008). Brittleness can also be characterized based on mineral composition, where Maende and Jarvie (2008) defined brittleness index as the content of brittle mineral quartz in rocks; quartz is a brittle mineral, and reservoirs with higher quartz content have higher fracability. The brittleness index method is simple to calculate and operationally feasible, but it only considers the potential for reservoirs to form fracture networks and cannot reflect the

hydrocarbon content of reservoirs.

Currently, the mainstream method for evaluating reservoir fracability involves the comprehensive analysis of the relationship between various influencing factors and production, and the establishment of a multi-parameter fracability evaluation coefficient (Jin et al., 2014; Guo et al., 2022). Different scholars choose different parameters for evaluating fracability, which can be divided into two main categories: geological influencing parameters and engineering influencing parameters. Jin et al. (2014) established a fracability evaluation model based on the critical strain energy release rate of reservoir core fracture extension and the brittleness index of reservoir core. Wang et al. (2015) considered the brittleness index, fracture density, and stress sensitivity as the main factors affecting reservoir fracability, which were firstly used as basic parameters for fracability evaluation, and calculated the fracability index of reservoirs accordingly. Sui et al. (2016) separately considered six influencing factors including clay mineral content, brittleness index, and uniaxial compressive strength on fracability, thereby establishing a fracability evaluation model with six evaluation parameters. Due to the fact that marine hydrate reservoirs are composed of loose sediment particles and hydrate particles with cohesive properties, and they possess characteristics such as shallow burial depth, weak/unconsolidated, and non-lithification, the fracturing behavior of hydrate reservoirs exhibits certain uniqueness. Therefore, it is an urgent issue to establish a fracability evaluation method suitable for hydrate reservoirs.

Currently, there are few reports on the assessability of hydraulic fracability of natural gas hydrate reservoirs. Liu et al. (2022b) conducted hydraulic fracturing experiments on different types of hydrate sediment, considering the influence of hydrate saturation, brittleness index, clay content, and differential stress. They established an assessment model for the fracability of hydrate reservoirs based on the analytic hierarchy process (AHP) and entropy method (EM), proposing criteria for evaluating the applicability of hydraulic fracturing in hydrate reservoirs based on fractureability index, fracturing fluid viscosity, and flow rate. Liu et al.'s research has made significant progress in evaluating the fracability of hydrate reservoirs, positively contributing to the assessment of hydraulic fracturing in hydrate reservoirs (Liu et al., 2022b). However, the study still faces some limitations. Firstly, the use of the AHP in the study to determine the weights of each parameter involves subjective judgments and blindness as it requires the subjective determination of the relative importance between factors. Although the EM was used to correct the weights in AHP, it still cannot overcome the fundamental flaw of subjective determination of variable importance, which is a current technical bottleneck in the evaluation of reservoir fracability. Secondly, the study did not provide a method for determining the sensitivity of each influencing factor to the changes in fracability; instead, it qualitatively specified the importance of each influencing factor, lacking quantitative research on the influencing factors.

To address the aforementioned issues, this study has defined the concept of fracability for both geological and engineering aspects of hydrate reservoirs. Based on the results of hydrate hydraulic fracturing experiments, the study quantitatively calculates the weights of various influencing factors using the grey relational analysis method. It then combine the criteria importance through intercriteria correlation (CRITIC) method to construct a comprehensive evaluation model for the fracability of hydrate reservoirs, which is highly applicable and objective. This paper is organized as follows: (1) we established a comprehensive geological-engineering evaluation model for the fracability of hydrate reservoirs in the chapter; (2) we introduced the true triaxial hydraulic fracturing experiment of hydrate sediments and the experimental results; (3) we applied the hydrate reservoir fracturability evaluation model in

combination with the experimental results and compared them with the results of previous studies; (4) we put forward conclusions and suggestions in Section 6. This model has engineering significance for selecting sweet spots for hydraulic fracturing in hydrate reservoirs, designing fracturing construction schemes, predicting and evaluating fracturing effects, among other engineering guidance purposes.

2. The comprehensive geological-engineering evaluation model for the fracability of hydrate reservoirs

2.1. Comprehensive fracability index

Generally speaking, from the perspective of geological factors, regions with abundant oil and gas resources and favorable physical properties are considered as the material basis for efficient reservoir development, emphasizing the innate conditions of reservoirs for development potential. From the perspective of engineering factors, regions conducive to the formation of complex fractures after fracturing are regarded as the technical guarantee for efficient reservoir development, emphasizing the potential for reservoirs to be modified post-development. Therefore, the concept of fracability itself encompasses both geological and engineering implications: only in areas with significant reservoir reserves and favorable geological conditions can economically viable gas flow be generated from the formation of complex fractures through fracturing operations. To accurately characterize and quantify geological and engineering fracability, the definitions of geological fracability index and engineering fracability index for hydrate reservoirs are established: regions with higher geological fracability index have better hydrate formation and reservoir physical conditions; similarly, the engineering fracability index represents the extent to which existing fracturing techniques can generate fractures and achieve maximum volume of hydrate reservoir modification. The overlapping area of geological and engineering fracability indices is defined as the comprehensive fracability index of the reservoir, as shown in Fig. 1.

2.2. Evaluation parameters for the fracability of hydrate reservoirs

2.2.1. Geological evaluation parameters

2.2.1.1. Porosity. Porosity is an extremely important parameter in reservoir evaluation. The greater the reservoir porosity, the more natural gas hydrate content is available at the same hydrate saturation. This implies more decomposable hydrate and higher gas production efficiency. Consequently, the higher the value of fracturing and exploitation. The impact of porosity on the fracability of

hydrates can be represented by ϕ .

2.2.1.2. Hydrate saturation. There are primarily three distribution patterns of hydrates within sediments: pore-filling suspension, contact cementation, and skeleton support. At low hydrate saturations, hydrates mainly suspend in dispersed form within the skeletal pores, known as the pore-filling suspension type, with weak reservoir cementation. As hydrate saturation increases, hydrate particles with cohesive properties act as "bridges" between loose sediment particles. Hydrate particles can become part of the sediment framework (Winters et al., 2004). Therefore, hydrate saturation is an important parameter influencing the physical and mechanical properties of hydrate reservoirs. The impact of saturation on the fracability of hydrates can be represented by S_{hy} .

$$S_{hy} = \frac{V_{hy}}{V} \quad (1)$$

where V_{hy} and V respectively represent the volume of hydrates and the volume of reservoir pores, m^3 .

2.2.2. Engineering evaluation parameters

2.2.2.1. Burial depth. The greater the burial depth, the higher the vertical stress, making it more difficult for fractures to initiate and propagate. The effect of burial depth on fracability can be reflected by the vertical stress, denoted by σ_v .

2.2.2.2. Differential stress. The initiation and propagation of hydraulic fractures require overcoming the combined constraints of rock tensile strength and differential stress. Fractures generally tend to propagate perpendicular to the direction of minimum horizontal principal stress. In hydraulic fracturing of shale formations with weak planes, it is generally believed that the smaller the stress anisotropy, the better the fracturing effect (Tang et al., 2011). This is because under lower stress differentials, hydraulic fractures are more likely to propagate along both the matrix and weak planes, forming complex fractures. In contrast, natural weak planes are not developed in hydrate reservoirs, and the degree of stress anisotropy is greater, making fractures more likely to propagate along dominant planes. Therefore, the influence of differential stress on hydraulic fracturing in hydrate reservoirs can be represented by the coefficient of horizontal stress differential (K).

$$K = \frac{\sigma_H - \sigma_h}{\sigma_h} \quad (2)$$

where σ_H represents the maximum horizontal principal stress, MPa; σ_h represents the minimum horizontal principal stress, MPa.

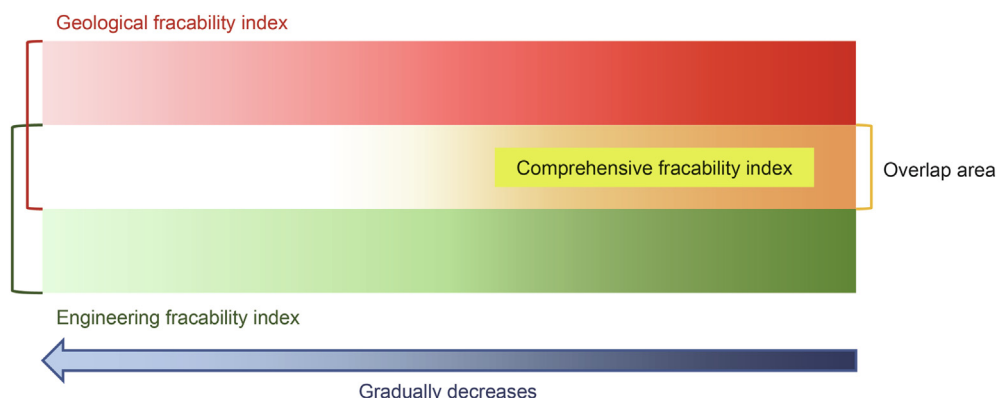


Fig. 1. Schematic diagram of comprehensive fracability index.

2.2.2.3. Brittleness index. Rock brittleness refers to an inherent property exhibited by rocks during stress-induced failure. It is generally defined as the ease of transient changes in rocks before rupture occurs and can be quantitatively characterized by a brittleness index. The brittleness index is a key indicator for evaluating the mechanical properties of reservoirs, with reservoirs having higher brittleness indices typically exhibiting better fracability. The dimensionless brittleness index (*BI*) can be characterized based on the elastic modulus and Poisson's ratio of rocks as proposed by Rickman et al. (2008).

$$BI = \frac{E_n + \mu_n}{2} \quad (3)$$

$$E_n = \frac{E - E_{\min}}{E_{\max} - E_{\min}} \quad (4)$$

$$\mu_n = \frac{\mu_{\max} - \mu}{\mu_{\max} - \mu_{\min}} \quad (5)$$

where *BI* is the brittleness index; E_n is the normalized elastic modulus, GPa; μ_n is the dimensionless normalized Poisson's ratio; E is the static elastic modulus, GPa; μ is the static Poisson's ratio; E_{\max} and E_{\min} are the maximum and minimum static elastic modulus of the target formation in GPa, respectively; μ_{\max} and μ_{\min} are the maximum and minimum static Poisson's ratio of the target formation, respectively.

2.2.2.4. Mineral composition. Hydrate reservoirs commonly contain a certain amount of clay components, and the mineral composition differences in hydrate reservoirs can significantly affect their fracability. Clay and other plastic mineral components are not conducive to the initiation and propagation of hydraulic fractures, while reservoirs with high contents of brittle minerals such as quartz, feldspar, and calcite are more prone to fracture during hydraulic fracturing processes. Maende and Jarvie (2008) proposed a mineral composition index (B_w) based on the content of brittle minerals per unit volume of rock.

$$B_w = \frac{W_{\text{calcite}} + W_{\text{feldspar}} + W_{\text{quartz}}}{W_{\text{all}}} \quad (6)$$

where w_{calcite} , w_{feldspar} , and w_{quartz} are the mass of calcite, feldspar, and quartz in the hydrate-bearing sediments components, respectively, kg; w_{all} is the mass of all mineral components, kg.

2.3. Data standardization processing

The units and dimensions of the six parameters (porosity, hydrate saturation, vertical stress, coefficient of horizontal stress differential, brittleness index, and mineral composition index) are all different, which can affect the accuracy of data analysis and evaluation results. It is necessary to normalize these parameters to maintain consistency. The differential transformation method can be used to standardize the parameters, including forward and reverse indicators (Zhao et al., 2017; Guo et al., 2020a).

The forward index is expressed as

$$S = \frac{X - X_{\min}}{X_{\max} - X_{\min}} \quad (7)$$

The reverse index is presented as

$$S = \frac{X_{\max} - X}{X_{\max} - X_{\min}} \quad (8)$$

where S is the standardized value of the evaluation parameter, dimensionless; X is the value of the evaluation parameter; X_{\max} and X_{\min} are the maximum and minimum values of the evaluation parameters in the target sediment, respectively.

2.4. Geological-engineering fracability index model

The fracability index is divided into geological fracability index and engineering fracability index. The fracability index integrates the influences of various factors, obtained by weighting the standardized evaluation parameters with coefficient weights. The calculation formula is

$$\begin{cases} w_G = \phi^S \cdot \lambda_\phi + S_{\text{hy}}^S \cdot \lambda_S \\ w_E = \sigma_v^S \cdot \lambda_v + K^S \cdot \lambda_K + BI^S \cdot \lambda_{BI} + B_w^S \cdot \lambda_B \end{cases} \quad (9)$$

where w_G represents the geological fracability index; and w_E represents the engineering fracability index; ϕ^S , S_{hy}^S , σ_v^S , K^S , BI^S , B_w^S are the evaluation parameters after standardization; λ_ϕ , λ_S , λ_v , λ_K , λ_{BI} , λ_B are the weight coefficients corresponding to the evaluation parameters.

Weights represent the relative importance of parameters contributing to the overall value, and their accuracy directly affects the evaluation effectiveness. Currently, there are many methods for determining weights, each with its own characteristics and applicability. The most commonly used method for determining weight coefficients is the AHP. However, AHP requires experts to make judgments and comparisons during the weight determination process, making it susceptible to subjective factors. Different experts may have different preferences and judgments, leading to uncertainty in the results. Moreover, if the user lacks detailed geological and engineering data for the evaluation area, it may result in significant deviations between the analysis results and the actual reservoir performance.

Therefore, in order to objectively and quantitatively calculate the weights of each evaluation parameter, a comprehensive weight model combining grey relational analysis and criteria importance through intercriteria correlation (CRITIC) methods is proposed. The grey relational analysis method compares and analyzes multiple parameters to determine the relative impact of several discrete functions on the objective function (Wang et al., 2023). This method has the advantages of simple calculation and insensitivity to small sample sizes (Wang, 2012). Simultaneously, the CRITIC method is introduced to evaluate the internal and intercriteria correlations. Based on this, a comprehensive weight calculation model suitable for evaluating the fracability of hydrate reservoirs is proposed, as elaborated below.

2.4.1. Grey relational analysis

Define Δ_{ij} as the deviation between the standardized j th evaluation parameter x_{ij} of the i th sample and the evaluation standard y_j

$$\Delta_{ij} = |x_{ij} - y_j|, \quad i = 1, 2, \dots, n; \quad j = 1, 2, \dots, m \quad (10)$$

The grey relational coefficient r_{ij} between the j th evaluation parameter of the i th sample and the evaluation standard is defined as

$$r_{ij} = \frac{\min_a \min_b \Delta_{ab} + \rho \max_a \max_b \Delta_{ab}}{\Delta_{ij} + \rho \max_a \max_b \Delta_{ab}} \quad (11)$$

where $a = 1, 2, \dots, n$; $b = 1, 2, \dots, m$; ρ is the resolution coefficient, typically taken as 0.5 (Han et al., 2024).

Taking the average of the grey relational coefficients r_{ij} for the j th evaluation parameter, we obtain the grey relational coefficient ε_j between the j th evaluation parameter and the evaluation standard.

$$\varepsilon_j = \frac{r_{ij}}{\sum_{i=1}^n r_{ij}}, \quad j = 1, 2, \dots, m \quad (12)$$

In this method, the evaluation standard is determined by calculating the ratio of the fracture area (the area of fracture extension divided by the cross-sectional area of the sample), denoted as R , based on the results of hydraulic fracturing experiments conducted on hydrate reservoirs.

2.4.2. CRITIC method

According to the CRITIC method, c is defined as the information content of indicators in the evaluation system. Therefore, the information content of the j th evaluation indicator is

$$c_j = s_j \sum_{k=1}^m (1 - \rho_{jk}), \quad j = 1, 2, \dots, m \quad (13)$$

where s_j represents the standard deviation of the j th evaluation indicator, indicating the internal contrast strength of the individual evaluation indicator; ρ_{jk} represents the correlation coefficient between evaluation indicators j and k .

When c_j is larger, it indicates that the j th evaluation index contains more information, and its corresponding weight should be higher. So, the objective weight ω_j of the j th indicator is given by

$$\omega_j = c_j / \sum_{k=1}^m c_k, \quad j = 1, 2, \dots, m \quad (14)$$

2.4.3. Comprehensive weight calculation

Considering the combined influence of grey relational analysis and the CRITIC method, after obtaining the grey relational coefficient ε_j and the CRITIC weight ω_j , normalization analysis is performed on both. The formula for calculating the comprehensive weight λ_j of the j th evaluation indicator is

$$\lambda_j = \varepsilon_j \omega_j / \left(\sum_{i=1}^n \varepsilon_i \omega_i \right) \quad (15)$$

2.5. Determination of comprehensive fracability index

The methods described above can be used to obtain the geological fracability index and the engineering fracability index. The relationship function between the two and the comprehensive fracability index is given by

$$FI = \alpha \cdot w_G + \beta \cdot w_E \quad (16)$$

where FI represents the fracability index; α and β are the weights related to geological and engineering fracability indexes, respectively, and obtained using a method based on multiple regression.

The fracture area ratio (R) is selected as the target parameter, and the linear correlation between R , w_G and w_E is established. The regression coefficients e and f in the formula are determined by multiple regression method, and then α and β are calculated.

$$R = e \cdot w_G + f \cdot w_E + g \quad (17)$$

$$\begin{cases} \alpha = \frac{e}{e+f} \\ \beta = \frac{f}{e+f} \end{cases} \quad (18)$$

3. Hydraulic fracturing experiments under true triaxial stress conditions for hydrate sediment

Evaluation of the fracability of hydrate reservoirs requires the integration of comprehensive fracability index and hydraulic fracturing experimental results. Initially, hydrate sediment samples are constructed, and their physical and mechanical properties are tested. Subsequently, hydraulic fracturing experiments are conducted.

3.1. Testing of the physical and mechanical properties of hydrate sediment

The testing of physical and mechanical properties of hydrate sediment primarily focuses on parameters such as porosity, elastic modulus, and Poisson's ratio. Porosity is measured using gas measurement methods, with the aim of calculating the volume of pores in hydrate sediment. This calculation allows for the determination of the amount of tetrahydrofuran (THF) and water required for different hydrate saturation levels based on the experimentally designed hydrate saturation. Elastic modulus and Poisson's ratio are obtained through shear experiments using an in-situ hydrate sediment triaxial mechanical parameter measurement device (Guo et al., 2014, 2020b).

The hydrate sediment is composed of pure natural quartz sand with a skeletal density of 2.65 g/cm³, with particle sizes ranging from 0.089 to 0.104 mm, serving as the medium for hydrate occurrence. To simulate two types of hydrate sediment, namely unconsolidated clayey silt hydrate sediment and weakly consolidated clayey silt hydrate sediment, different amounts of clay (composed of montmorillonite, kaolinite, and illite in a mass ratio of 7:2:1) and lime are added to the quartz sand. To expedite hydrate formation and enhance experimental efficiency, THF is used as the hydrate-forming agent. The hydrate formation temperature is set to 1 °C to ensure it is above the freezing point of water, avoiding interference from ice formation during the experiment. A low-temperature and high-pressure environment for THF hydrate formation is established. During shearing, the system is maintained at a stable temperature of 1 °C to prevent hydrate decomposition.

3.2. Hydraulic fracturing experiments on hydrate sediment

In the hydraulic fracturing experiments on hydrate sediment, the same formula as that used for the skeletal framework in the shear experiments on hydrate sediment is utilized to construct the fracturing samples. Based on the skeletal volume and the measured skeletal porosity, the amount of tetrahydrofuran required for different hydrate saturations is calculated, and tetrahydrofuran solution is prepared accordingly. The skeletal framework is immersed in the prepared mixed solution for saturation.

Subsequently, the framework is wrapped with rubber film, subjected to two cycles of temperature elevation and reduction, and then placed in the sample holder. The cold storage temperature is set to 1 °C and maintained for 24 h, with nitrogen gas introduced to a pressure of 4.5 MPa to ensure the completion of tetrahydrofuran hydrate formation. Through this process, two types of fracturing samples are created: unconsolidated clayey silt hydrate sediment and weakly consolidated clayey silt hydrate sediment, which respectively simulate hydrate reservoirs in marine clayey silt and permafrost regions. The hydraulic fracturing experiments on hydrate sediment employ a self-developed low-temperature true triaxial hydraulic fracturing simulation experimental system (Fig. 2). The specific experimental scheme is outlined in Table 1.

Based on the proportions of components such as quartz sand, clay, and lime in the hydrate sediment, the mineral composition index can be calculated. The elastic modulus and Poisson's ratio obtained from the triaxial shear experiments on hydrate sediment can be used to calculate the brittleness index of the hydrate sediment. The vertical stress and the calculation of the horizontal stress differential coefficient can be obtained based on the triaxial stress settings in the hydraulic fracturing experiments.

Fig. 3 shows the fracturing results of the unconsolidated clayey silty sand hydrate sediment. No crosslinker was added to the samples, relying solely on hydrate bonding and the cohesion between clay and silt sand. The samples contain a certain amount of clay components, exhibiting low elastic modulus, high Poisson's ratio, and strong plasticity overall. Among the four sets of samples (No. 1, No. 3, No. 4, and No. 6) subjected to low flow rates (5 mL/min) for fracturing, no fractures were formed. The fracturing fluid infiltrated the samples in a seepage form, resulting in substantial loss and causing clay component mudification within the sample. Particularly, severe mudification occurred around the wellbore, leading to sediment deformation, reduced bonding strength, and even wellbore collapse. The other six sets of samples were fractured by increasing either the fluid volume (up to 20 mL/min) or viscosity (up to 240 mPa s), resulting in the formation of fractures with varied morphologies.

Fig. 4 depicts the fracturing results of the weakly cemented clayey silty sand hydrate sediment. Taking sample No. 11 as an example, clear fractures and fracturing fluid outflow were observed along the boundary in the direction of the maximum principal

stress. However, the rock-breaking process caused the sample to fragment, making it impossible to showcase the interior of the fractures. The other six sets of samples all formed fractures with varying morphologies after fracturing.

4. Application of the hydrate reservoir fracability evaluation model

4.1. Calculation of model parameters

Based on the principle of controlling variables, under the conditions of fracturing fluid viscosity of 30 mPa s and fracturing fluid flow rate of 10 mL/min, four samples (No. 2, No. 9, No. 19, and No. 20) were selected. Utilizing computer image processing technology, the fracture area ratio (R) of the samples was calculated. Firstly, the distribution of surface fractures on the samples after fracturing was observed, and then the samples were cut along the surface fractures. Next, the extent of internal hydraulic fracture expansion was observed, and the fracture expansion surface was intercepted. Image grayscale processing was performed, converting it into a binary image with pixels only in white (representing unexpanded areas) and black (representing expanded areas). Finally, the ratio of black pixels N_f to total pixels N_s was calculated to obtain the fracture area ratio. The specific operational procedures and results are shown in Fig. 5.

The results of grey relational analysis, CRITIC method, and the comprehensive weight calculation of each parameter are shown in Table 2. Based on Eq. (17), the regression equation for geological and engineering fracability indices with fracture area ratio is obtained as follows:

$$R = 0.2231 \cdot w_G + 0.222 \cdot w_E + 0.289 \quad (19)$$

According to Eq. (18), α and β are calculated as 0.51 and 0.49, respectively. Finally, the formula for calculating the fracability index is obtained as

$$FI = 0.51 (0.8344S_{hy} + 0.1656\phi) + 0.49(0.0683\sigma_v + 0.2022K + 0.6830BI + 0.0466B_w) \quad (20)$$

4.2. Assessment of hydrate reservoir fracability

Eq. (20) is applied to calculate the fracability index of the 20 sets of hydrate sediment samples as shown in Table 3. Since the injection volume of fracturing fluid is controlled to be very small during the experiment, it cannot directly guide field practice. The experimental flow rate is converted from the injection volume according to the wellbore diameter, calculated as follows:

$$v = \frac{q}{A} \quad (21)$$

where v represents the flow velocity of the fracturing fluid inside the wellbore, m/s; q represents the pumping rate of the fracturing fluid, m³/s; A represents the cross-sectional area of the wellbore, m².

According to Table 3, when the geological fracability indices are similar, a higher engineering fracability index corresponds to a greater feasibility of forming fractures in gas hydrate sediments during fracturing operations, resulting in a larger comprehensive fracability index, FI (samples No. 4, No. 5, No. 6, No. 14, No. 17, and No. 20). Overall, the FI determined by the intrinsic properties of gas hydrate sediments plays a crucial role in their fracability. However,

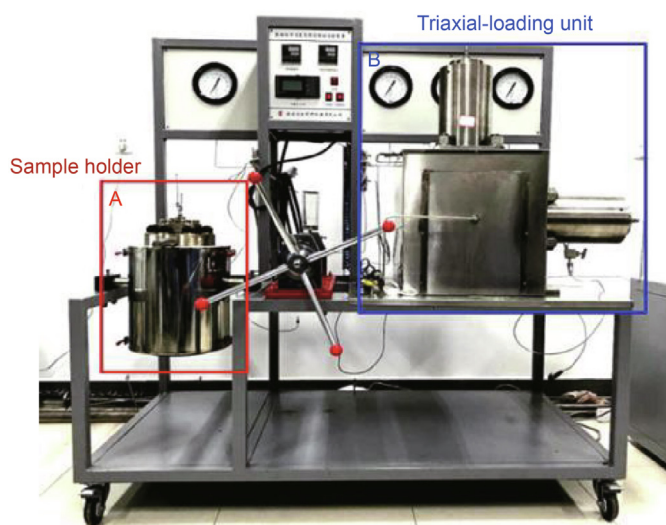


Fig. 2. Low temperature resistance true triaxial hydraulic fracturing simulation test system.

Table 1
Hydrate sediment hydraulic fracturing experimental plan.

No.	Type of hydrate sediment	Vertical stress $\sigma_v/\sigma_H/\sigma_h$, MPa	Hydrate saturation	Fracturing fluid volume, mL/min	Fracturing fluid viscosity, mPa s	
1	Unconsolidated clayey silty sand hydrate sediment	8/6/4	10	5	120	
2				10	30	
3			30	5	30	
4					120	
5					240	
6			50		5	1
7					10	
8					20	
9					10	30
10			50		10	30
11	Weakly consolidated clayey silty sand hydrate sediment	8/6/4	10	10	30	
12				5	1	
13			30		15	
14					30	
15					45	
16			50		10	30
17					3	
18					10	30
19					10	30
20				7/6/4	10	10
		7/6/3	30			

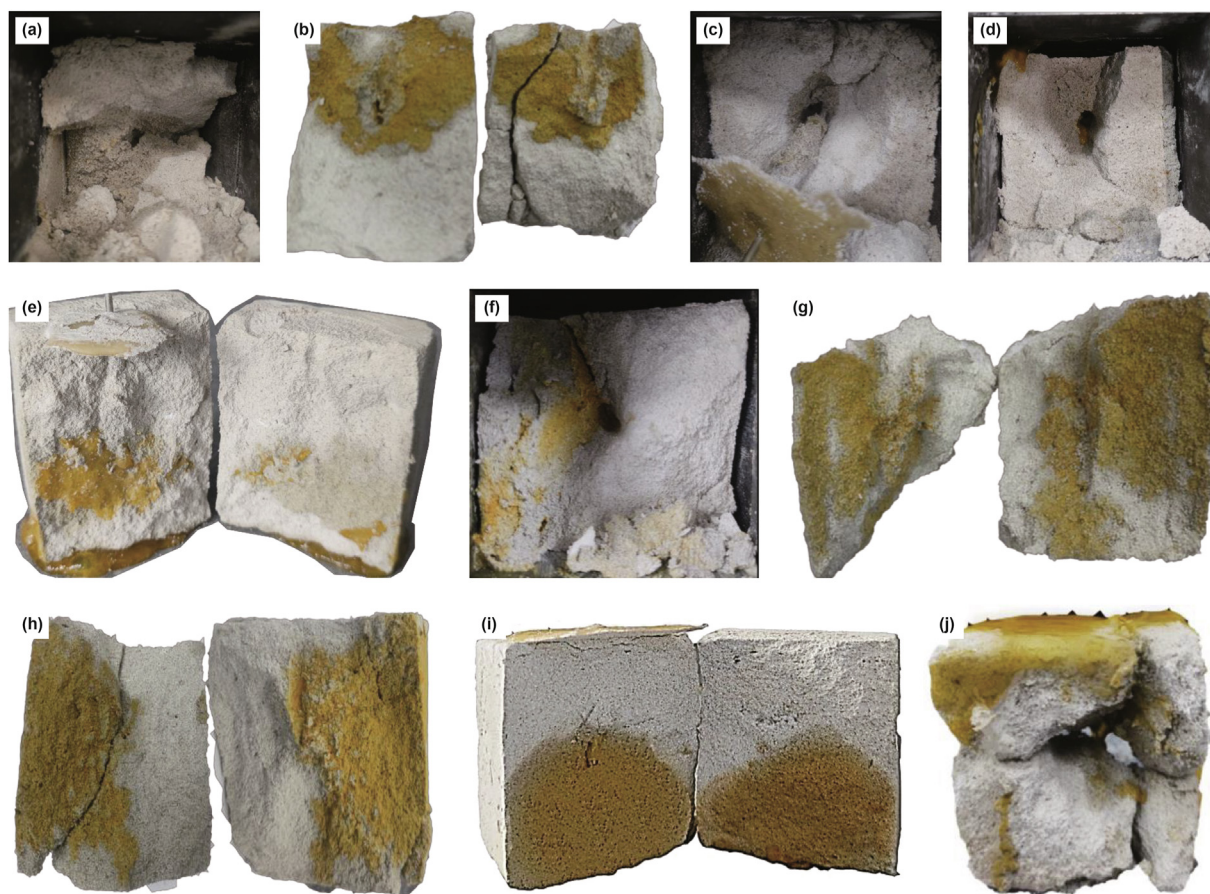


Fig. 3. The fracturing results of the unconsolidated clayey silty sand hydrate sediment are shown in (a)–(j) for samples No. 1 to No. 10.

taking samples No. 2, No. 3, and No. 4 as examples, although $FI_{No. 2}$ is lower than $FI_{No. 3}$ and $FI_{No. 4}$, fissures formed after fracturing sample No. 2, while samples No. 3 and No. 4 did not form fissures. This

indicates that the fracability of gas hydrate sediments is not only related to fracability indices but also closely related to construction parameters such as fracturing fluid viscosity and pumping rate.

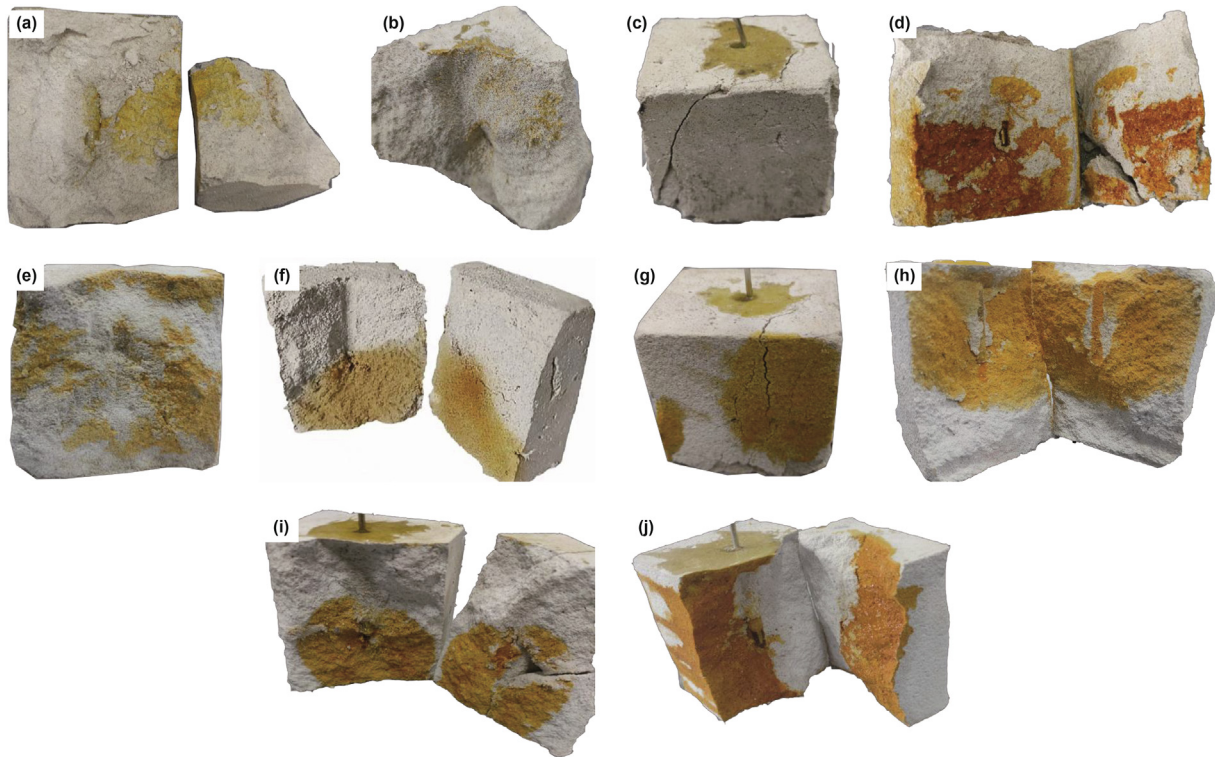


Fig. 4. The fracturing results of the weakly cemented clayey silty sand hydrate sediment are shown in (a)–(j) for samples No. 11 to No. 20.

Sample No. 11 has a lower FI compared to sample No. 12. However, both the fracturing fluid viscosity and pumping rate of sample No. 11 are greater than those of sample No. 12. After fracturing, sample No. 11 formed fissures, while sample No. 12 did not. It appears that increasing the fracturing fluid viscosity and pumping rate can aid in fissure formation. When comparing sample No. 2 ($FI = 0.12$, with fissures) to sample No. 1 ($FI = 0.11$, without fissures), although their FI values are similar, the fracturing fluid viscosity of sample No. 2 decreased by 75%, and the pumping rate increased by 50%. Fissures formed after fracturing, indicating that the impact of pumping rate on the fracability of gas hydrate sediments is greater than that of fracturing fluid viscosity.

To investigate the influence of fracturing construction parameters on the fracturing effectiveness of gas hydrate sediments, a comprehensive characterization method for fracturing construction parameters was established based on multiple linear regression. Firstly, the data of pumping rate (v) and fracturing fluid viscosity (u) were standardized. The correlation function between the normalized fracturing construction parameters $\bar{v}\bar{u}$ and v and u is defined as

$$\bar{v}\bar{u} = \delta \cdot v + \eta \cdot u \quad (22)$$

where $\bar{v}\bar{u}$ represents the normalized fracturing construction parameters; δ and η respectively represent the weights associated with pumping rate and fracturing fluid viscosity.

Select the fracturing outcome (F) as the target parameter, where 1 indicates the presence of fractures and 0 indicates their absence. Establish a linear correlation equation between F , FI , fracturing fluid velocity (v), and fracturing fluid viscosity (u). Using multiple regression analysis, determine the regression coefficients h , i , and j in the equation, and then calculate δ and η .

$$F = o \cdot FI + p \cdot v + s \cdot u + t \quad (23)$$

$$\begin{cases} \delta = \frac{p}{p+s} \\ \eta = \frac{s}{p+s} \end{cases} \quad (24)$$

According to the results in Table 3, regression based on Eq. (23) yields the following equation:

$$F = 1.112FI + 1.274v + 0.563u - 0.196 \quad (25)$$

According to Eq. (24), the calculated values of δ and η are 0.69 and 0.31, respectively. The results indicate that the influence of fracturing fluid velocity on the fracturing outcome is higher than that of fracturing fluid viscosity, consistent with the observed pattern in the experiments. The final formula for normalized fracturing construction parameters is

$$\bar{v}\bar{u} = 0.69v + 0.31u \quad (26)$$

Based on Eq. (26), the value of parameter $\bar{v}\bar{u}$ for 20 sets of gas hydrate sediment samples is calculated. The compressibility of gas hydrate sediment samples with different FI under different values of $\bar{v}\bar{u}$ according to the comprehensive fracability index and the results of fracturing tests, is shown in Fig. 6.

According to Fig. 6, as the FI increases, the value of $\bar{v}\bar{u}$ required for gas hydrate sediment samples to fracture gradually decreases, reflecting that sediment samples with higher FI exhibit better fracability. Additionally, for each FI , there should be a critical $\bar{v}\bar{u}'$ under which fracturing conditions ($\bar{v}\bar{u} \geq \bar{v}\bar{u}'$) allow the sediment samples to fracture, while conditions ($\bar{v}\bar{u} < \bar{v}\bar{u}'$) do not. This critical

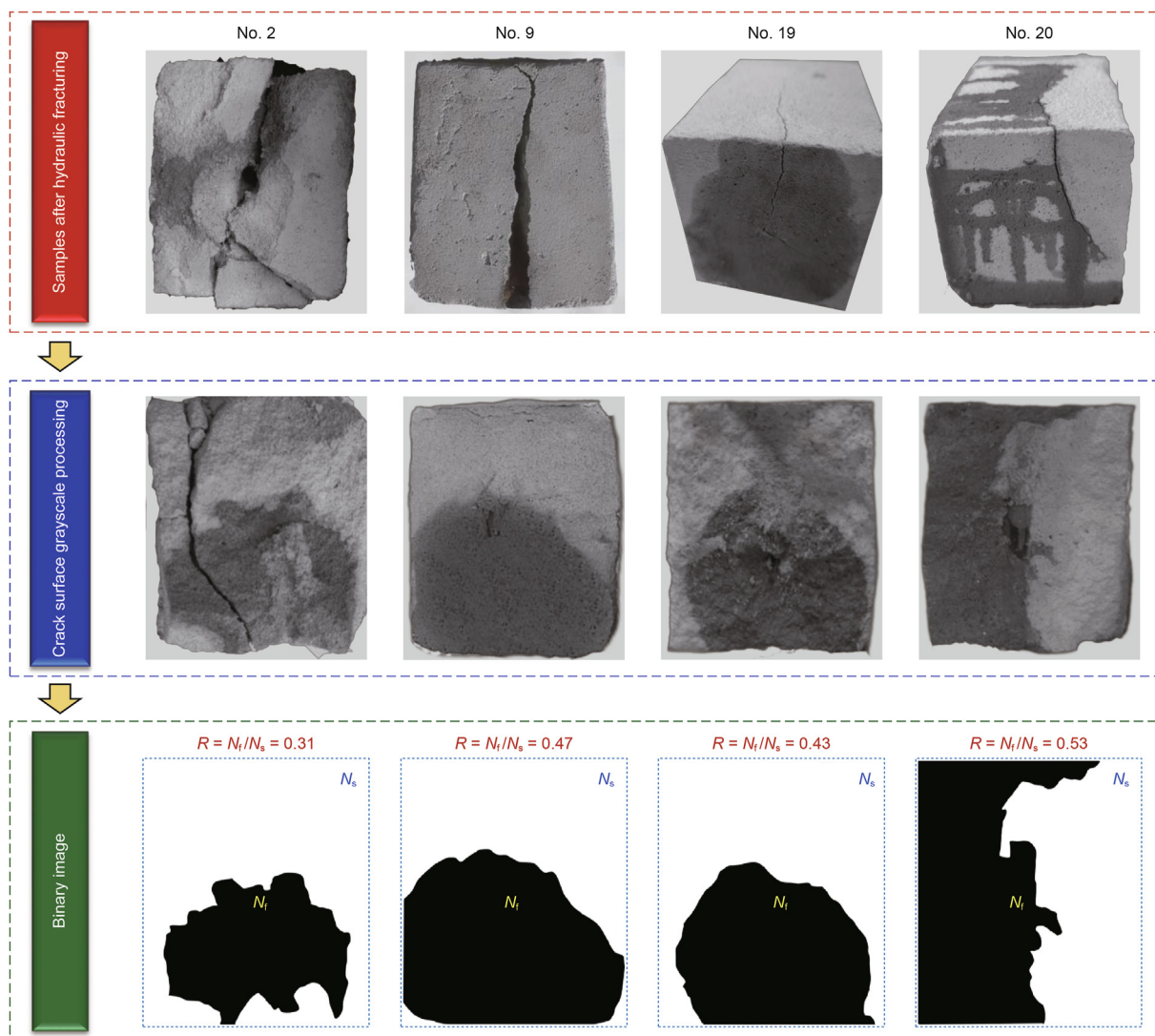


Fig. 5. The calculation procedure and results of the fracture area ratio.

Table 2
The weight calculation results.

Method	Geological parameter		Engineering parameter			
	Hydrate saturation	Porosity	Vertical stress	Horizontal stress differential coefficient	Brittleness index	Mineral composition index
Grey relational analysis	0.7809	0.5755	0.4279	0.5688	0.9666	0.7220
CRITIC	0.7879	0.2121	0.1240	0.2765	0.5494	0.0501
Comprehensive weight	0.8344	0.1656	0.0683	0.2022	0.6830	0.0466

relationship is depicted as a curve in the graph, defined as the critical construction parameter curve. To find this critical construction parameter curve, various regression forms (logarithmic, exponential, linear, and polynomial regression) were attempted based on experimental results to regress FI and $\bar{v}u'$. Different regression results are shown in Fig. 6.

According to the linear regression results (Fig. 7(c)), when FI is greater than 0.8, $\bar{v}u'$ displays as a negative value. However, the range of $\bar{v}u'$ should be within $[0, 1]$, so the critical construction parameter curve obtained by linear regression is numerically unreasonable. According to the polynomial regression results (Fig. 7(d)), with the increase of FI , $\bar{v}u'$ exhibits a feature of first

decreasing and then increasing, which does not match the trend obtained from the experiment. Therefore, the critical construction parameter curve obtained by polynomial regression is physically unreasonable.

Comparing the results of logarithmic regression and exponential regression (Fig. 7(a) and (b)), the values of $\bar{v}u'$ obtained by both methods within the range $FI \in [0, 1]$ are greater than 0, and the trend decreases gradually with the increase of FI , which conforms to the experimental law. For $FI \in (0, 0.1)$, there is no experimental evidence for the trend. However, based on experimental laws and common knowledge, when $FI \rightarrow 0$, the sediment sample of gas hydrate tends towards being unfracturable, meaning that fractures cannot be generated under any fracturing construction parameters.

Table 3
Fracability index and fracturing outcome.

Type of hydrate sediment	No.	E , GPa	μ	v , 10^{-2} m/s	u , mPa s	S_{Hy}	ϕ	BI	B_w	σ_v	K	w_G	w_E	FI	Result
Unconsolidated clayey silty sand hydrate sediment	1	0.68	0.36	8	120	0.1	0.37	0.00	0.7	7	0.5	0.08	0.13	0.11	No fracture
	2	0.69	0.36	16	30	0.1	0.36	0.00	0.7	7	0.5	0.10	0.14	0.12	Fracture
	3	0.81	0.35	8	30	0.3	0.35	0.03	0.7	7	0.5	0.29	0.15	0.22	No fracture
	4	0.83	0.36	8	120	0.3	0.34	0.04	0.7	7	0.5	0.29	0.16	0.22	No fracture
	5	0.82	0.35	8	240	0.3	0.35	0.11	0.7	7	0.5	0.29	0.21	0.25	Fracture
	6	0.85	0.36	8	1	0.3	0.35	0.04	0.7	7	0.5	0.29	0.16	0.22	No fracture
	7	0.86	0.35	16	1	0.3	0.34	0.12	0.7	7	0.5	0.31	0.22	0.26	Fracture
	8	0.85	0.34	32	1	0.3	0.34	0.20	0.7	7	0.5	0.31	0.27	0.29	Fracture
	9	0.87	0.35	16	30	0.3	0.34	0.12	0.7	7	0.5	0.31	0.22	0.26	Fracture
	10	1.41	0.33	16	30	0.5	0.32	0.41	0.7	7	0.5	0.51	0.41	0.46	Fracture
Weakly consolidated clayey silty sand hydrate sediment	11	2.21	0.33	16	30	0.1	0.32	0.58	0.8	7	0.1	0.18	0.46	0.31	Fracture
	12	2.72	0.32	8	1	0.3	0.31	0.78	0.8	7	0.5	0.36	0.67	0.51	No fracture
	13	2.71	0.32	8	15	0.3	0.32	0.78	0.8	7	0.5	0.34	0.67	0.50	No fracture
	14	2.83	0.30	8	30	0.3	0.31	0.97	0.8	7	0.5	0.38	0.80	0.59	Fracture
	15	2.73	0.33	8	45	0.3	0.33	0.70	0.8	7	0.5	0.32	0.61	0.47	Fracture
	16	2.78	0.31	16	30	0.3	0.3	0.88	0.8	7	0.5	0.38	0.74	0.55	Fracture
	17	2.81	0.30	4.8	30	0.3	0.32	0.97	0.8	7	0.5	0.38	0.80	0.58	No fracture
	18	2.97	0.30	16	30	0.5	0.28	1.00	0.8	7	0.5	0.58	0.82	0.70	Fracture
	19	2.21	0.33	16	30	0.1	0.32	0.58	0.8	6	0.5	0.18	0.61	0.39	Fracture
	20	2.81	0.31	16	30	0.3	0.3	0.88	0.8	6	1.0	0.38	0.91	0.64	Fracture

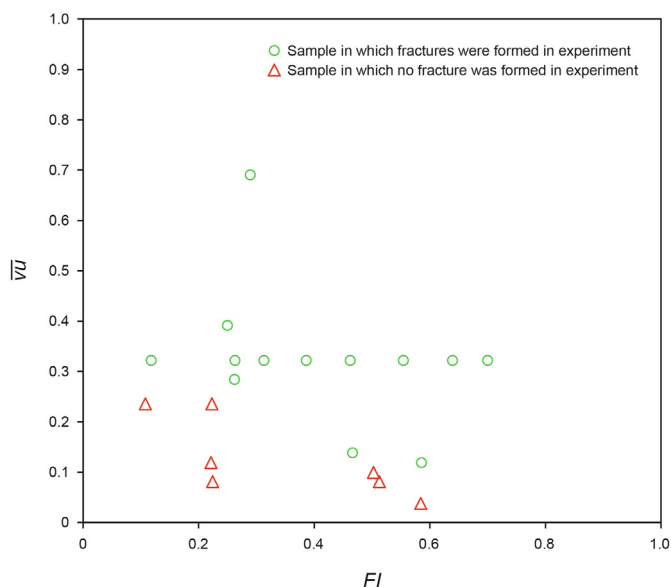


Fig. 6. $\bar{v}u'$ calculation results.

The corresponding $\bar{v}u'$ will tend towards infinity. However, the results of exponential regression indicate that $FI \rightarrow 0: \bar{v}u' = 0.41$, while the results of logarithmic regression indicate that $FI \rightarrow 0: \bar{v}u' \rightarrow \infty$. Therefore, based on the above analysis, it is concluded that the result obtained by logarithmic regression is the critical construction parameter curve, with its calculation formula as follows:

$$\bar{v}u' = -0.129 \ln(FI) + 0.0451 \tag{27}$$

where $\bar{v}u'$ represents the critical normalized hydraulic fracturing construction parameter.

In practical applications, the comprehensive fracability index FI of gas hydrate reservoirs can be calculated using a geological-engineering comprehensive evaluation model. Then, according to Eq. (26), the normalized critical hydraulic fracturing construction parameter $\bar{v}u'$ can be obtained. By comparing it with the actual hydraulic fracturing construction parameters calculated for $\bar{v}u$, one

can determine whether fracturing can occur.

4.3. Gas hydrate reservoir fracability chart

To rapidly assess the fracability of gas hydrate reservoirs, a two-dimensional fracability index evaluation chart is established based on experimental results and the correlation between geological fracability index, engineering fracability index, and comprehensive fracability index as described in Section 2.5. This chart is shown in Fig. 8. In practical applications, the w_G and w_E of gas hydrate reservoirs can be calculated using Eq. (20) and then projected onto the two-dimensional fracability index evaluation chart. This allows for a rapid quantitative assessment of their fracability: the larger the w_G , the more "worthwhile" the reservoir is for fracturing, while the larger the w_E , the more "feasible" it is to fracture the reservoir.

Additionally, based on this, on-site practitioners can flexibly define and delineate comprehensive fracability zones. For instance, setting $FI = 0.5$ as the lower limit of the comprehensive fracability zone in advance, when the FI of a reservoir is located in the region above the contour line representing $FI = 0.5$, the fracability of this gas hydrate reservoir meets the development requirements.

Upon completing the identification of gas hydrate reservoir fracability and determining the fracturing construction parameters, to facilitate rapid on-site assessment of whether fractures can be induced in the reservoir under the chosen fracturing conditions, a three-dimensional fracturing construction condition discrimination chart for gas hydrate reservoirs has been established, as shown in Fig. 9. In practical applications, after determining the FI of the reservoir and the critical construction parameter $\bar{v}u$, they are projected onto the three-dimensional fracturing construction condition discrimination chart. If the projected point lies above the purple surface, it indicates that fractures can be induced in the reservoir under the selected fracturing construction conditions.

4.4. Model comparison and evaluation

Applying the GC model from this study and the AE model (Liu et al., 2022b), we calculated the fracturability of samples in Experiment A and Experiment B (Liu et al., 2022b) to assess whether the samples could form fractures, the results are shown in Table 4.

The calculated results of FI and $\bar{v}u$ by the GC model for

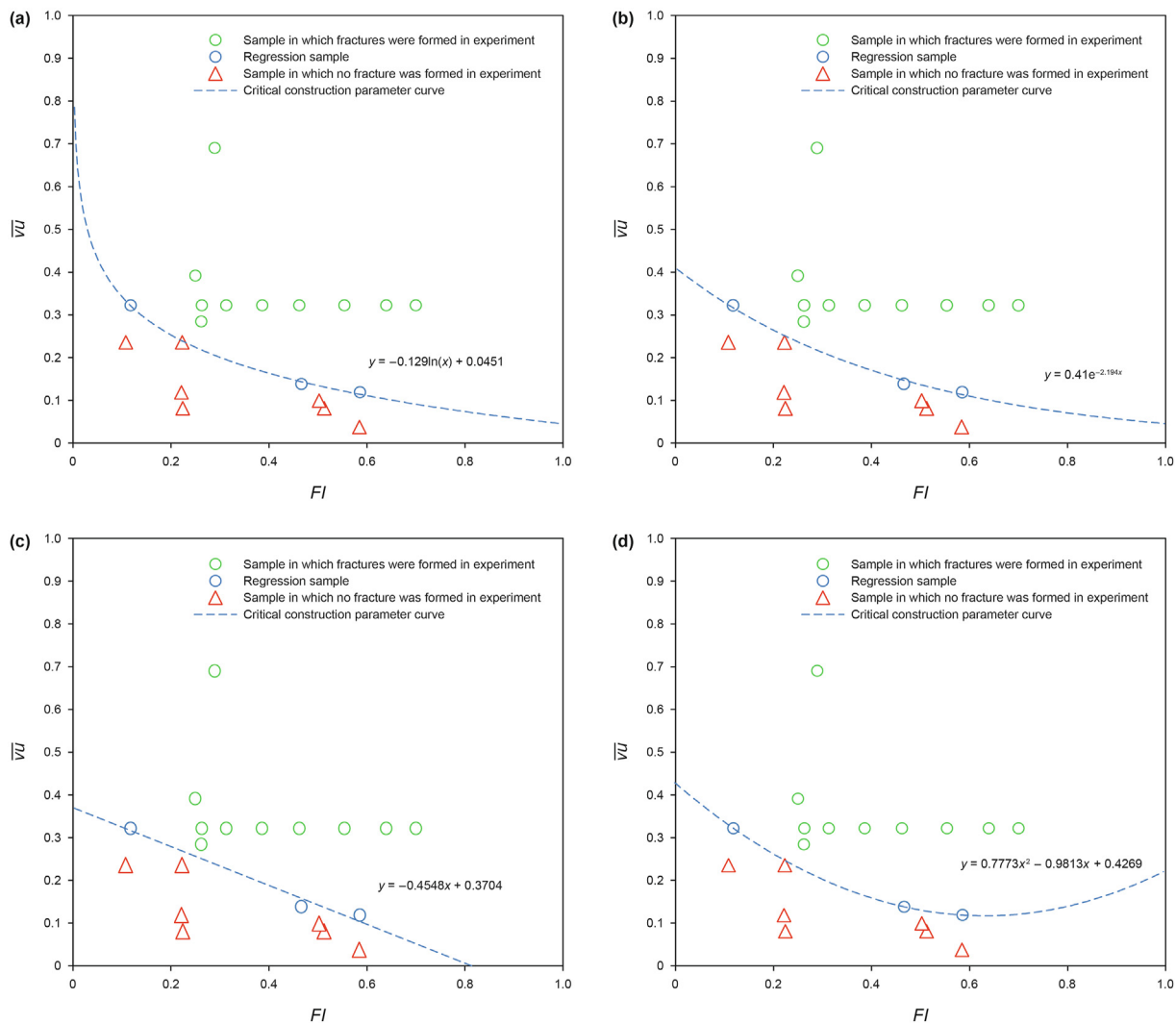


Fig. 7. Regression results of critical construction parameter curve: (a) logarithmic regression, (b) exponential regression, (c) linear regression, (d) polynomial regression.

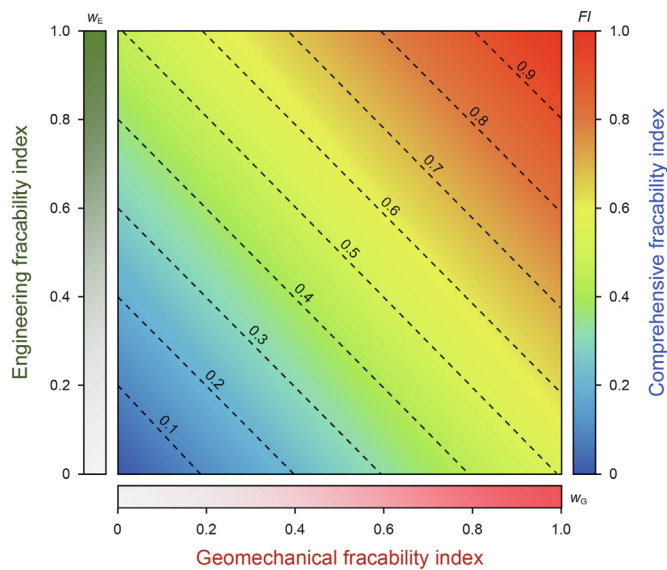


Fig. 8. Two-dimensional fracability index evaluation chart.

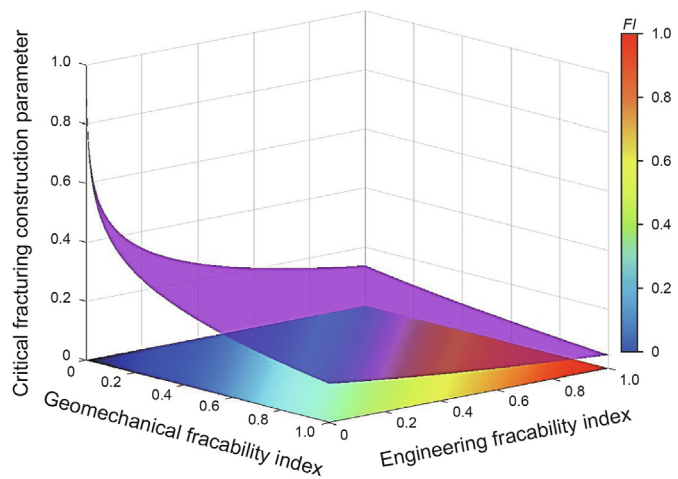


Fig. 9. Three-dimensional fracturing construction condition discrimination chart.

specimens in Experiment A and Experiment B, as well as the discrimination of fracturing results by the critical construction parameter curve, are shown in Fig. 10.

Table 4
Fracability index and fracturing results.

Experiment A				Experiment B			
No.	Fracturing result	Result of the GC model	Result of the AE model	No.	Fracturing result	Result of the GC model	Result of the AE model
1	No fracture	No fracture	Uncertain ☒	1	No fracture	No fracture	No fracture
2	Fracture	Fracture	Uncertain ☒	2	No fracture	No fracture	No fracture
3	No fracture	No fracture	Uncertain ☒	3	No fracture	No fracture	No fracture
4	No fracture	No fracture	Uncertain ☒	4	No fracture	No fracture	No fracture
5	Fracture	Fracture	Uncertain ☒	5	No fracture	No fracture	No fracture
6	No fracture	No fracture	Uncertain ☒	6	No fracture	No fracture	Uncertain ☒
7	Fracture	Fracture	Uncertain ☒	7	Fracture	No fracture ☒	Uncertain ☒
8	Fracture	Fracture	Uncertain ☒	8	No fracture	No fracture	Uncertain ☒
9	Fracture	Fracture	Uncertain ☒	9	No fracture	No fracture	Uncertain ☒
10	Fracture	Fracture	Uncertain ☒	10	Fracture	No fracture ☒	Fracture
11	Fracture	Fracture	Uncertain ☒	11	No fracture	No fracture	No fracture ☒
12	No fracture	No fracture	Uncertain ☒	12	No fracture	Fracture ☒	No fracture ☒
13	No fracture	No fracture	Uncertain ☒	13	Fracture	Fracture	Fracture
14	Fracture	Fracture	Uncertain ☒	14	Fracture	Fracture	Fracture
15	Fracture	No fracture ☒	Uncertain ☒	15	Fracture	Fracture	Fracture
16	Fracture	Fracture	Uncertain ☒	16	Fracture	Fracture	Fracture
17	No fracture	No fracture	Uncertain ☒	17	Fracture	Fracture	Fracture
18	Fracture	Fracture	Uncertain ☒	18	Fracture	Fracture	Fracture
19	Fracture	Fracture	Uncertain ☒	19	Fracture	Fracture	Fracture
20	Fracture	Fracture	Uncertain ☒				

When the model is uncertain about whether fractures are formed, it is defined as a misjudgment

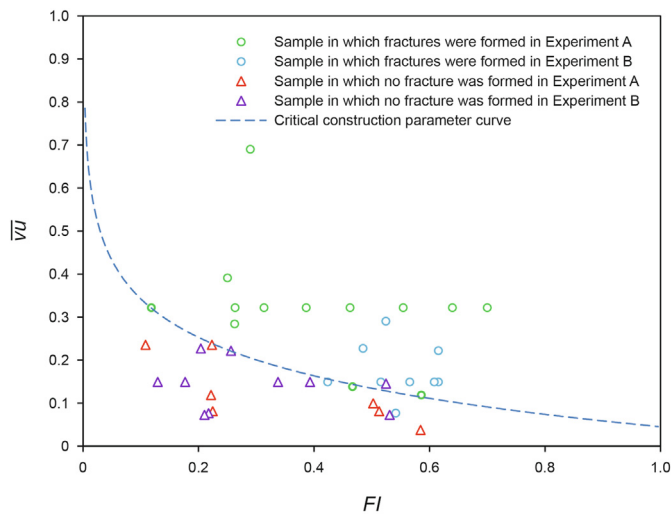


Fig. 10. The computed results of the GC model and AE model.

Considering the model's determination of whether fractures are formed in the specimen as a binary classification problem, the concept of a confusion matrix is introduced to compare the predicted results from the model with the actual results and categorize them into four scenarios (True positives: model assess the samples could form fractures and samples form fractures; False negatives: model assess the samples couldn't form fractures but samples form fractures; False positives: model assess the samples could form fractures but samples didn't form fractures; True negatives: model assess the samples couldn't form fractures and samples didn't form fractures) (Table 5) to evaluate the model performance. Evaluation metrics include accuracy, precision, recall, and F1 score.

(1) Accuracy (A)

Predicted correct samples as a percentage of the total, with the specific formula as follows:

Table 5
Confusion matrix table.

Actual label	Predicted label	
	Positive instances	Negative instances
Positive instances	TP (true positives)	FN (false negatives)
Negative instances	FP (false positives)	TN (true negatives)

$$A = \frac{TP + TN}{TP + FN + FP + TN} \times 100\% \tag{28}$$

(2) Precision (P)

An evaluation metric for predicted results, also known as precision. It measures the percentage of truly positive samples among those predicted as positive. The specific formula is as follows:

$$P = \frac{TP}{TP + FP} \times 100\% \tag{29}$$

(3) Recall (R)

An evaluation metric for the original samples, also known as recall. It measures the percentage of samples predicted as positive among the actual positive samples. The specific formula is as follows:

$$R = \frac{TP}{TP + FN} \times 100\% \tag{30}$$

(4) F1 score (F1)

F1 score is a harmonic mean that balances precision and recall. It is used to consider both metrics simultaneously. The specific

formula is as follows:

$$F1 = \frac{2 \times P \times R}{P + R} \times 100\% \tag{31}$$

Combining the results from Table 4 and Fig. 10, the calculated evaluation metrics for both the GC model and the AE model are presented in Table 6. The radar chart in Fig. 11 illustrates the performance comparison of the models. It can be observed that the GC model achieves accuracy, precision, recall, and F1 score all above 85%, while all evaluation metrics for the AE model are below 50%. This indicates that the model established in this paper can more accurately evaluate the fracability of gas hydrate reservoirs.

5. Application and limitation

This study established a comprehensive evaluation model of gas hydrate reservoir fracability from an objective perspective, determining the influence of various factors on the fracability of gas hydrate reservoirs. Further development of gas hydrate reservoir fracturing techniques was achieved, providing a theoretical basis for the design of gas hydrate reservoir fracturing schemes. The fracability chart developed in this research assists in flexibly defining and delineating comprehensive fracturing zones on-site, providing technical means for rapidly analyzing the fracability of gas hydrate reservoirs.

However, this study only used the fracture area ratio as an evaluation metric to quantitatively analyze the importance of various influencing factors. If production rates could be combined to calculate the weights of influencing factors, the results might be more objective and accurate. Currently, there is a lack of experimental analysis on gas hydrate reservoir fracturing production rates. It is recommended to improve experimental methods in the future to explore the impact of various factors on post-fracturing production in gas hydrate reservoirs and further optimize model weights.

6. Conclusions

This study has established a comprehensive evaluation model for the fracability of gas hydrate reservoirs based on grey relational analysis and the CRITIC method. By combining with hydraulic fracturing experiments on gas hydrate sediments, the fracability of gas hydrate reservoirs was evaluated. The specific research conclusions are as follows.

- (1) The concept of gas hydrate reservoir fracability is a comprehensive evaluation indicator of reservoir geological conditions and the difficulty level of fracturing construction. The importance of factors affecting geological fracability is ranked as follows (in brackets is the comprehensive weight): gas hydrate saturation (0.8344) > porosity (0.1656). The importance of factors affecting engineering fracability is ranked as follows: brittleness (0.6830) > horizontal stress

Table 6
Calculation results of evaluation metrics for two models.

Evaluation metrics	Calculation result	
	GC model	AE model
Accuracy, %	89.74	33.33
Precision, %	95.00	40.00
Recall, %	86.36	36.36
F1 score, %	90.48	38.10

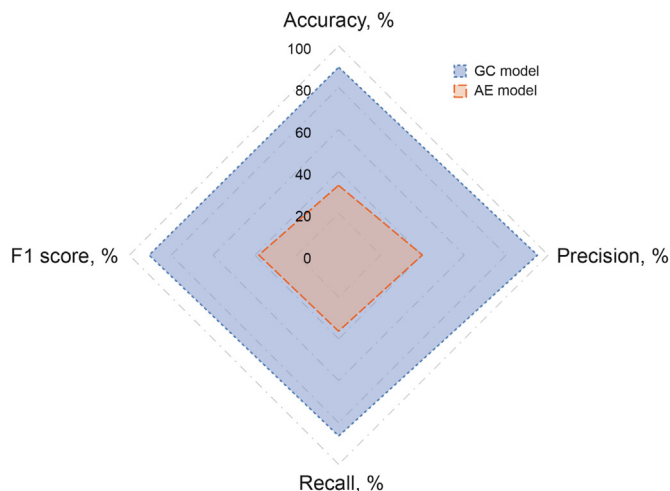


Fig. 11. Model performance comparison radar chart.

- difference coefficient (0.2022) > vertical geostress (0.0683) > mineral composition index (0.0466).
- (2) Normalized fracturing construction parameters were defined to comprehensively characterize the influence of construction parameters on the fracability of gas hydrate reservoirs. The impact of fracturing fluid flow rate (weight of 0.69) on whether fracturing forms fractures is higher than the impact of fracturing fluid viscosity (weight of 0.31). The concept of a critical construction parameter curve was first defined. Four regression results show that using logarithmic regression to calculate the critical construction parameter curve results in a better fit with experimental and physical laws. Overall, as the comprehensive fracability index increases, the feasibility of gas hydrate reservoir fracturing increases, and the fracturing fluid viscosity and volume required to generate fractures gradually decrease.
- (3) Based on experimental results, a two-dimensional fracability index evaluation chart was established, which can be used to flexibly define and delineate comprehensive fracturing zones: a larger w_G indicates a reservoir more "worthy" of fracturing, while a larger w_E indicates a reservoir more "easily" fractured. A three-dimensional fracturing construction condition discrimination chart was established based on the critical construction parameter curve, facilitating rapid on-site determination of whether fractures can be generated in the reservoir under the specified fracturing construction conditions.
- (4) The applicability of the comprehensive geological-engineering fracability evaluation model for gas hydrate reservoirs established in this study is good, with strong objectivity. It achieves rapid evaluation of whether gas hydrate reservoirs are worth fracturing, whether they are easily fractured, and whether they can be fractured. The accuracy rate of judging experimental results reaches 89.74%, which has engineering guidance significance for hydraulic fracturing in gas hydrate reservoirs.

CRedit authorship contribution statement

Tian-Kui Guo: Writing – review & editing, Validation, Supervision, Conceptualization. **Lin-Rui Xue:** Writing – original draft, Visualization, Methodology, Conceptualization. **Ming Chen:** Validation, Supervision, Methodology, Conceptualization. **Bo Zhang:**

Software, Resources, Formal analysis. **Zhen-Tao Li:** Investigation, Formal analysis, Data curation. **Wen-Jie Huang:** Validation, Resources, Methodology, Investigation. **Xiao-Qiang Liu:** Resources, Data curation. **Zhan-Qing Qu:** Investigation, Formal analysis, Data curation.

Declaration of competing interest

The authors declare that they have no known competing financial interests or personal relationships that could have appeared to influence the work reported in this paper.

Acknowledgments

The authors would like to acknowledge the financial support of the National Natural Science Foundation of China (Grant No. 52074332).

References

- Chen, L., Feng, Y.C., Okajima, J., et al., 2018. Production behavior and numerical analysis for 2017 methane hydrate extraction test of Shenhu, South China Sea. *J. Nat. Gas Sci. Eng.* 53, 55–66. <https://doi.org/10.1016/j.jngse.2018.02.029>.
- Chen, X.J., Lu, H.L., Gu, L.J., et al., 2022. Preliminary evaluation of the economic potential of the technologies for gas hydrate exploitation. *Energy* 243, 123007. <https://doi.org/10.1016/j.energy.2021.123007>.
- Cheng, F.B., Sun, X., Li, Y.H., et al., 2023. Numerical analysis of coupled thermal-hydro-chemo-mechanical (THCM) behavior to joint production of marine gas hydrate and shallow gas. *Energy* 281, 128224. <https://doi.org/10.1016/j.energy.2023.128224>.
- Chong, K.K., Grieser, W.V., Passman, A., et al., 2010. A completions guide book to shale-play development: a review of successful approaches towards shale-play stimulation in the last two decades. In: Canadian Unconventional Resources and International Petroleum Conference. <https://doi.org/10.2118/133874-MS>.
- De Silva, V.R.S., Ranjith, P.G., Perera, M.S.A., et al., 2019. Artificial fracture stimulation of rock subjected to large isotropic confining stresses in saline environments: application in deepsea gas hydrate recovery. *Nat. Resour. Res.* 28 (2), 563–583. <https://doi.org/10.1007/s11053-018-9409-0>.
- Guo, T.K., Zhang, S.C., Qu, Z.Q., et al., 2014. Experimental study of hydraulic fracturing for shale by stimulated reservoir volume. *Fuel* 128, 373–380. <https://doi.org/10.1016/j.fuel.2014.03.029>.
- Guo, T.K., Zhang, S.C., Ge, H.K., et al., 2015. A new method for evaluation of fracture network formation capacity of rock. *Fuel* 140, 778–787. <https://doi.org/10.1016/j.fuel.2014.10.017>.
- Guo, T.K., Li, Y.C., Ding, Y., et al., 2017. Evaluation of acid fracturing treatments in shale formation. *Energy Fuels* 31 (10), 10479–10489. <https://doi.org/10.1021/acs.energyfuels.7b01398>.
- Guo, T.K., Tang, S.J., Sun, J., et al., 2020a. A coupled thermal-hydraulic-mechanical modeling and evaluation of geothermal extraction in the enhanced geothermal system based on analytic hierarchy process and fuzzy comprehensive evaluation. *Appl. Energy* 258, 113981. <https://doi.org/10.1016/j.apenergy.2019.113981>.
- Guo, T.K., Tang, S.J., Liu, S., et al., 2020b. Physical simulation of hydraulic fracturing of large-sized tight sandstone outcrops. *SPE J.* 26 (1), 372–393. <https://doi.org/10.2118/204210-PA>.
- Guo, D.L., Zhang, S.L., Wang, X., et al., 2022. Comprehensive evaluation of coalbed fracability based on dynamic weight function. *Journal of Southwest Petroleum University (Science & Technology Edition)* 44 (2), 97–104. <https://doi.org/10.11885/j.issn.1674-5086.2020.08.07.01> (in Chinese).
- Ge, K., Liu, J.X., Wang, J.Q., et al., 2023. Numerical simulation of gas production behavior of class I, class II and class III hydrate reservoirs for different well locations. *J. Clean. Prod.* 433, 139844. <https://doi.org/10.1016/j.jclepro.2023.139844>.
- Han, S., Li, D., Li, K., et al., 2024. Analysis and study of transmission line icing based on grey correlation Pearson combinatorial optimization support vector machine. *Measurement* 115086. <https://doi.org/10.1016/j.measurement.2024.115086>.
- Ito, T., Igarashi, A., Suzuki, K., et al., 2008. Laboratory study of hydraulic fracturing behavior in unconsolidated sands for methane hydrate production. In: Offshore Technology Conference. <https://doi.org/10.4043/19324-MS>.
- Jin, X.C., Shah, S.N., Roegiers, J.C., et al., 2014. Fracability evaluation in shale reservoirs—an integrated petrophysics and geomechanics approach. In: SPE Hydraulic Fracturing Technology Conference and Exhibition. <https://doi.org/10.2118/168589-MS>.
- Konno, Y., Jin, Y., Yoneda, J., et al., 2016. Hydraulic fracturing in methane-hydrate-bearing sand. *RSC Adv.* 10, 73148–73155. <https://doi.org/10.1039/C6RA15520K>.
- Kurihara, M., Sato, A., Funatsu, K., et al., 2010. Analysis of production data for 2007/2008 Mallik gas hydrate production tests in Canada. In: SPE International Oil and Gas Conference and Exhibition in China. <https://doi.org/10.2118/132155-MS>.
- Liu, W.G., Song, Q., Wu, P., et al., 2023. Triaxial tests on anisotropic consolidated methane hydrate-bearing clayey-silty sediments of the South China Sea. *Energy* 284, 129260. <https://doi.org/10.1016/j.energy.2023.129260>.
- Liu, X.Q., Qu, Z.Q., Guo, T.K., et al., 2021. A coupled thermo-hydrologic-mechanical (THM) model to study the impact of hydrate phase transition on reservoir damage. *Energy* 216, 119222. <https://doi.org/10.1016/j.energy.2020.119222>.
- Liu, X.Q., Sun, Y., Guo, T.K., et al., 2022a. Numerical simulations of hydraulic fracturing in methane hydrate reservoirs based on the coupled thermo-hydrologic-mechanical-damage (THMD) model. *Energy* 238, 122054. <https://doi.org/10.1016/j.energy.2021.122054>.
- Liu, X.Q., Guo, T.K., Qu, Z.Q., et al., 2022b. Fracability evaluation model and application of hydraulic fracturing in natural gas hydrate reservoir. *Journal of Central South University (Science and Technology)* 53 (3), 1058–1068. <https://doi.org/10.11817/j.issn.1672-7207.2022.03.026> (in Chinese).
- Lu, C., Qin, X.W., Mao, W.J., et al., 2021. Experimental study on the propagation characteristics of hydraulic fracture in clayey-silt sediments. *Geofluids* 1468–8115. <https://doi.org/10.1155/2021/6698649>.
- Ma, X.L., Jiang, D.D., Sun, Y.H., et al., 2022. Experimental study on hydraulic fracturing behavior of frozen clayey silt and hydrate-bearing clayey silt. *Fuel* 322, 124366. <https://doi.org/10.1016/j.fuel.2022.124366>.
- Maende, A., Jarvie, D., 2008. Finding bypassed or overlooked pay zones using geochemistry techniques. In: International Petroleum Technology Conference. <https://doi.org/10.2523/IPTC-12918-MS>.
- Qu, Z.Q., Tian, Y., Li, J.X., et al., 2017. Numerical simulation study on fracture extension and morphology of multi-cluster staged fracturing for horizontal wells. *J. China Univ. Petrol. (Edn. Nat. Sci.)* 41, 102–109. <https://doi.org/10.3969/j.issn.1673-5005.2017.01.013> (in Chinese).
- Rick, R., Mike, M., Erik, P., et al., 2008. A practical use of shale petrophysics for stimulation design optimization: all shale plays are not clones of the Barnett shale. In: SPE Annual Technical Conference and Exhibition. <https://doi.org/10.2118/115258-MS>.
- Rickman, R., Mullen, M.J., Petre, E., et al., 2008. A practical use of shale petrophysics for stimulation design optimization: all shale plays are not clones of the Barnett Shale. In: SPE Annual Technical Conference and Exhibition. <https://doi.org/10.2118/115258-MS>. Denver, Colorado, USA, 2008: SPE-115258-MS.
- Schoderbek, D., Farrell, H., Howard, J., et al., 2013. ConocoPhillips Gas Hydrate Production Test: NT0006553. ConocoPhillips Co., Houston <https://doi.org/10.2172/1123878>, 2013.
- Sloan, E., 2003. Fundamental principles and applications of natural gas hydrates. *Nature* 426, 353–359. <https://doi.org/10.1038/nature02135>.
- Sui, L.L., Ju, Y., Yang, Y.M., et al., 2016. A quantification method for shale friability based on analytic hierarchy process. *Energy* 115, 637–645. <https://doi.org/10.1016/j.energy.2016.09.035>.
- Sun, Y.F., Cao, B.J., Chen, H.N., et al., 2023. Influences of pore fluid on gas production from hydrate-bearing reservoir by depressurization. *Petrol. Sci.* 20 (2), 1238–1246. <https://doi.org/10.1016/j.petsci.2022.09.015>.
- Sun, Y.M., Li, S.D., Lu, C., et al., 2021. The characteristics and its implications of hydraulic fracturing in hydrate-bearing clay silt. *J. Nat. Gas Sci. Eng.* 95, 104189. <https://doi.org/10.1016/j.jngse.2021.104189>.
- Tang, S., Zhu, B., Yan, Z., 2011. Effect of crustal stress on hydraulic fracturing in coalbed methane wells. *J. China Coal Soc.* 36 (1), 65–69. <https://doi.org/10.13225/j.cnki.jccs.2011.01.005> (in Chinese).
- Too, J.L., Cheng, A., Khoo, B.C., et al., 2018. Hydraulic fracturing in a penny-shaped crack. Part II: testing the frackability of methane hydrate-bearing sand. *J. Nat. Gas Sci. Eng.* 52, 619–628. <https://doi.org/10.1016/j.jngse.2018.01.046>.
- Wang, B., Zhen, F., Zhao, J., et al., 2018. Influence of intrinsic permeability of reservoir rocks on gas recovery from hydrate deposits via a combined depressurization and thermal stimulation approach. *Appl. Energy* 229, 858–871. <https://doi.org/10.1016/j.apenergy.2018.08.056>.
- Wang, C., Du, H., Sun, X., et al., 2023. Comprehensive evaluation method of shale oil sweet spot based on grey correlation analysis: a case study of Bonan Sag in Bohai Bay Basin. *Petroleum Drilling Techniques* 51 (5), 130–138. <https://doi.org/10.11911/syztjs.2023085>. (in Chinese).
- Wang, D.B., Ge, H.K., Wang, X.Q., et al., 2015. A novel experimental approach for friability evaluation in tight-gas reservoirs. *J. Nat. Gas Sci. Eng.* 23, 239–249. <https://doi.org/10.1016/j.jngse.2015.01.039>.
- Wang, J., 2012. Evaluation of business performance of listed shipping companies: grey correlation analysis based on CRITIC method. *Management and Administration* (2), 94–96. <https://doi.org/10.16517/j.cnki.cn12-1034/f.2012.02.001> (in Chinese).
- Wei, J.G., Lin, Y., Liang, Q.Y., et al., 2021. Geomechanical properties of gas hydrate-bearing sediments in Shenhu area of the south China Sea. *Energy Rep.* 7, 8013–8020. <https://doi.org/10.1016/j.egyr.2021.05.063>.
- Winters, W.J., Pecher, I.A., Waite, W.F., et al., 2004. Physical properties and rock physics models of sediment containing natural and laboratory-formed methane hydrate. *Am. Mineral.* 89 (8), 1221–1227. <https://doi.org/10.2138/am-2004-8-909>.
- Yagiz, S., 2006. An investigation on the relationship between rock strength and brittleness. In: Proceedings of the 59th Geological Congress of Turkey. <https://www.jmo.org.tr/etkinlikler/kurultay/index.php?etkinlikkod=7>.
- Yamamoto, K., Terao, Y., Fujii, T., et al., 2014. Operational overview of the first offshore production test of methane hydrates in the Eastern Nankai Trough. In: Offshore Technology Conference. <https://doi.org/10.4043/25243-MS>.

Yang, L., Shi, F., Yang, J., 2020. Experimental studies on hydraulic fracturing in hydrate sediment. *Chem. Technol. Fuels Oils* 56, 107–114. <https://doi.org/10.1007/s10553-020-01116-8>.

Zhang, W.D., Shi, X., Jiang, S., et al., 2020. Experimental study of hydraulic fracture initiation and propagation in highly saturated methane-hydrate-bearing sands.

J. Nat. Gas Sci. Eng. 79 (77), 103338. <https://doi.org/10.1016/j.jngse.2020.103338>.

Zhao, H.L., Yao, L.H., Mei, G., et al., 2017. A fuzzy comprehensive evaluation method based on AHP and entropy for a landslide susceptibility map. *Entropy* 19 (8), 396. <https://doi.org/10.3390/e19080396>.